

Accelerating Dust Temperature Calculations with Graphics Processing Units

Patrik Jonsson, Joel R. Primack

Santa Cruz Institute for Particle Physics, University of California, Santa Cruz, CA 95064, USA

Abstract

When calculating the infrared spectral energy distributions (SEDs) of galaxies in radiation-transfer models, the calculation of dust grain temperatures is generally the most time-consuming part of the calculation. Because of its highly parallel nature, this calculation is perfectly suited for massively parallel general-purpose Graphics Processing Units (GPUs). This paper presents an implementation of the calculation of dust grain equilibrium temperatures on GPUs in the Monte-Carlo radiation transfer code SUNRISE, using the CUDA API. The GPU can perform this calculation 69 times faster than the 8 CPU cores, showing great potential for accelerating calculations of galaxy SEDs.

Key words: dust, radiative transfer, methods: numerical
PACS: 95.30.Jx, 98.38.Ca, 98.58.Jg, 95.75.Pq

1. Introduction

Over the last decade, radiation-transfer models of dust in galaxies have become increasingly capable, with higher spatial resolutions, higher wavelength resolutions, and more realistic descriptions of the dust itself (Gordon et al., 2001; Jonsson, 2006; Li et al., 2008; Bianchi, 2008; Chakrabarti and Whitney, 2009; Jonsson et al., 2009). Current codes calculate the temperatures of grains of a number of different compositions and sizes based on physical dust models (e.g. Weingartner and Draine, 2001; Draine and Li, 2007) at many different spatial locations in the problem, sometimes also including thermal fluctuations. As the complexity of the dust models have gone up, researchers have found that the most computationally demanding part of the calculation no longer is the actual transfer of radiation through the medium, but rather the calculation of the dust emission spectrum.

At the same time, graphics-processing units (GPUs) have evolved from specialty hardware to massively parallel general computation devices. These devices are made to render independent pixels, where the same computation is being done millions of times on largely independent data. The predictable data access pattern means that the considerable amount of silicon real estate which is used to hide memory latency on a general-purpose CPU is unnecessary. Instead, the entire chip area can be used for computational units, giving a raw floating-point processing power many times larger than that of CPUs of similar cost and power consumption.

The utility of GPUs for general high-performance computations was initially limited by the fact that programs needed to be expressed in terms of graphics operations and written in shading languages such as Cg or GLSL, making it difficult to port programs. Still, astrophysical applications were explored, for example N-body calculations (Portegies Zwart et al., 2007) with large increases in performance compared to custom GRAPE hardware. The programming obstacle was largely overcome with the Nvidia CUDA (Compute Unified Device Architecture, NVIDIA Corporation, 2009b) API, which enables programs to be written in a language very similar to C/C++, with added directives. CUDA has been used in astrophysics not only for N-body calculations (Belleman et al., 2008; Gaburov et al., 2009) but also for radio interferometer data processing (Ord et al., 2009) and exoplanet searches (Ford, 2009), to name a few.

This paper presents an implementation of the dust grain equilibrium temperature and emission SED calculation in CUDA for the Monte-Carlo radiation transfer code SUNRISE (Jonsson, 2006; Jonsson et al., 2009). The CUDA version obtains a speedup of more than two orders of magnitude compared to a modern CPU core when using an Nvidia Tesla C1060 high-performance computing card. We start by outlining the calculation and the CUDA implementation in Sections 2 – 4, present accuracy tests and benchmarks in Section 5, and conclude with a discussion and summary in Sections 6 & 7.

2. The Calculation of Dust Emission

SUNRISE, a radiation-transfer code using the Monte-Carlo method to calculate the transfer of light through a dusty medium, has been described in previous papers.

*Corresponding author. Present address: Harvard-Smithsonian Center for Astrophysics, 60 Garden St., MS-51, Cambridge, MA 02138, USA. Tel.: +1 (617) 384-7831, fax: +1 (617) 495-7093

Email addresses: pjonsson@cfa.harvard.edu (Patrik Jonsson), joel@scipp.ucsc.edu (Joel R. Primack)

The basic computational algorithm was described in Jonsson (2006), and the computation of dust emission, along with results from an application of the code to hydrodynamic simulations of spiral galaxies, in Jonsson et al. (2009). SUNRISE is free software and the source code, including the CUDA implementation used here, is available on the SUNRISE home page.¹ The calculation of the dust emission spectra, detailed in e.g. Misselt et al. (2001), is reviewed here to set the stage for implementing this calculation in CUDA.

In the simplest calculation of emission from dust grains, each grain is simply assumed to emit like a modified blackbody, the temperature of which can be found by equating the emitted luminosity with the luminosity L_h heating the grain (normally assumed to result from absorption of shorter-wavelength radiation, but in principle from any source, for example heating by high-energy electrons). This leads to the equation

$$L_h = \int \sigma_a(\lambda) B(\lambda, T_e) d\lambda = 2hc^2 \int \frac{\sigma_a(\lambda)}{(e^{hc/(k\lambda T_e)} - 1) \lambda^5} d\lambda, \quad (1)$$

which needs to be solved numerically to find the equilibrium temperature T_e . In this formula, $\sigma_a(\lambda)$ is the (wavelength-dependent) absorption cross section of the dust grain, $B(\lambda, T)$ is the blackbody function, and c , h , and k are the speed of light and the constants of Planck and Boltzmann. Once the equilibrium temperature is known, the dust emission spectrum $L_{\lambda,e}$ can be calculated as

$$L_{\lambda,e}(\lambda) = \sigma_a(\lambda) B(\lambda, T_e). \quad (2)$$

Because a solution to Equation 1 is necessary for a number of dust grains of different sizes and compositions in a number of different grid cells with different intensities of the heating radiation, Equation 1 needs to be solved on the order of hundreds of millions of times to calculate the dust emission in one of the simulation snapshots to which SUNRISE is typically applied. To show this more explicitly, the subscripts s and c are used to indicate that the quantities depend on the dust grain species (size and composition) and grid cell, respectively. The calculations necessary can then be summarized by the following equations:

$$L_{h;c,s} = \int I_c(\lambda) \sigma_{a;s}(\lambda) d\lambda \quad (3)$$

$$L_{h;c,s} = 2hc^2 \int \frac{\sigma_{a;s}(\lambda)}{(e^{hc/(k\lambda T_{e;c,s})} - 1) \lambda^5} d\lambda \quad (4)$$

$$L_{\lambda,e;c,s}(\lambda) = \sigma_{a;s}(\lambda) B(\lambda, T_{e;c,s}) \quad (5)$$

The need for a numerical solution to Equation 4, using on the order of 1000 wavelength bins, and the fact that a global iterative procedure is necessary to find the equilibrium distribution of radiative intensities in cases where

the dust is optically thick to its own radiation (see Jonsson et al., 2009), means that calculating the dust emission involves the evaluation of at least $10^{11} - 10^{12}$ exponentials. Evaluating an exponential is one of the most computationally costly mathematical operations to perform on a modern CPU, and this explains the large computational cost of the calculation. Indeed, in a typical SUNRISE run, the time for the dust emission calculation outweighs the time for the transfer of radiation by a large factor. (For the case used to produce the results in Section 5, the temperature calculation takes $\sim 90\%$ of the total time, and this generally increases further for cases with more complicated geometry and higher optical depth.) Since operations with high floating-point intensity are good candidates for porting to a GPU due to their large advantage in raw floating-point power, this indicates that performing the calculation on the GPU has a large potential speedup.

The seasoned computationist will at this point argue that this reasoning may be correct but ultimately irrelevant, as the sensible way of calculating T_e many times is by setting up a lookup table of $T_{e;s}(L_{h;s})$, thus bypassing the numerical solution of Equation 4. This is true (and is how the calculation is actually performed in SUNRISE), but proceeding with the GPU implementation is useful, for several reasons. First, as will be shown below, the exact calculation of $L_e(\lambda)$ performed on the GPU *is actually faster than a temperature table interpolation implemented on the CPU*, a remarkable fact in itself. Second, the implementation of the calculation of *equilibrium* temperature emission serves as a useful warm-up for implementing the calculation of grains with *fluctuating* temperatures (as outlined in e.g. Guhathakurta and Draine, 1989), which is even more computationally intensive.

3. The CUDA Programming Model

The CUDA programming model consists of functions, called *kernels*, that are meant to execute on the GPU. When the host CPU starts a kernel, it is executed simultaneously for a large number of threads. These threads are divided into *blocks*, where threads in the same block can communicate through a comparatively small amount of shared, high-speed memory. On the current generation of hardware (CUDA compute model 1.3), a block can consist of up to 1024 threads. Threads in different blocks cannot communicate and are completely independent.

The actual hardware consists of an array of execution units called Streaming Multiprocessors. Each multiprocessor executes one (or several) thread blocks concurrently. The set of threads that executes simultaneously, called a *warp*, on current hardware is 32. Within a warp, the threads execute one common instruction at a time, but with individual data. Out of the currently executing threads, the hardware schedules warps with zero overhead, so warps that are unable to execute because they are waiting for loads from the (uncached) global memory will yield the hardware to other warps that are ready to execute.

¹The SUNRISE home page is <http://sunrise.familjenjonsson.org>.

The performance concerns for writing GPU programs are enumerated in the CUDA “Best Practices Guide” (NVIDIA Corporation, 2009a). Two of the most important concerns of an efficient GPU algorithm are: first, minimizing access to the (uncached) global memory by staging data in the fast shared memory to avoid unnecessary loads and making sure loads are *coalesced*. For a coalesced load, all threads in the two halves of a warp perform their loads in one memory transaction (unlike uncoalesced loads which require several – up to 16 – memory transactions and can thus take up to 16 times longer). The criteria for coalesced loads vary between device generations, and the C1060 hardware used here can coalesce all loads where threads access memory within the same 128-byte segment (for loads of 4-byte data). Because of the large potential performance impact of uncoalesced loads, care has to be taken when designing the memory access pattern of the kernels.

The second important concern is the hiding of the global memory latency by maintaining high concurrency (NVIDIA Corporation, 2009b). If the number of concurrent warps executing is high enough, warps waiting for global memory can always be substituted for others that are ready to execute. The number of blocks that can execute concurrently on a multiprocessor is determined by the number of processor registers and the amount of shared memory used by the kernel, so minimizing use of these resources is important for maintaining high concurrency.

4. The CUDA Temperature Calculation

With the above background, it is now clear that the dust temperature calculation is well suited for a GPU implementation. The calculation consists of millions of identical, independent evaluations of Equations 3 – 5. Each CUDA thread will calculate the temperature and emission SED of a particular dust grain species in a particular grid cell.

If the integrals in Equations 3 – 5 are replaced with the finite-difference equivalent sums that will actually be calculated, the result is

$$L_{h;c,s} = \sum_l I_{c,l} \sigma_{a;s,l} \Delta\lambda_l \quad (6)$$

$$L_{h;c,s} = 2hc^2 \sum_l \frac{\sigma_{a;s,l} \Delta\lambda_l}{(e^{hc/(k\lambda_l T_{e;c,s})} - 1) \lambda_l^5} \quad (7)$$

$$L_{\lambda,e;c,s,l} = \sigma_{a;s,l} B(\lambda_l, T_{e;c,s}) \quad (8)$$

where l is the index used for the wavelength-dependent quantities.

In addition, after calculating the emission spectra of the individual grains in a grid cell, the total emission in a grid cell needs to be calculated by summing over the different grain species in the cell. Combining this sum

with Equation 8 yields

$$L_{\lambda,e;c,l} = \sum_s L_{\lambda,e;c,s,l} n_s m_{d;c} \quad (9)$$

$$= \sum_s \frac{2hc^2 \sigma_{a;s,l} n_s m_{d;c}}{(e^{hc/(k\lambda_l T_{e;c,s})} - 1) \lambda_l^5}. \quad (10)$$

where n_s is the number of dust grains of species s per unit mass of dust, and m_d is the mass of dust in the grid cell.

The calculation is performed with 4 kernels: The first kernel precomputes the quantity $\sigma_{a;s,l} \Delta\lambda_l$, which is used in Equations 6 & 7. The second kernel calculates the heating luminosity $L_{h;c,s}$. The third solves Equation 7 for the equilibrium temperature $T_{e;c,s}$. The fourth kernel calculates $L_{\lambda,e;c,l}$ using Equation 10.

The thread blocks have specific sizes, such as 16 elements of s and 8 elements of l , and the actual number of cells, dust species and wavelengths may not be evenly divisible by the block size. For this reason, the problem is padded with zeros so no edge checks are necessary in the kernels.

All GPU calculations use single-precision floating point numbers. While the GT200 architecture does have double-precision support, the double-precision performance is a small fraction of that using single-precision. As shown in Section 5, the use of single precision does not significantly affect the computed results. However, care must be taken to avoid under- or overflowing the limited dynamic range, as astrophysical numbers can span ranges rivaling that of single-precision numbers.

The GPU also has a fast intrinsic function for calculating exponentials in one clock cycle, `__expf`. This function has lower accuracy than the math library function `expf`, but is much faster. It was verified that using `__expf` had no adverse impact on the accuracy of the SED calculation, but resulted in about 40% higher overall performance, so the results presented here use `__expf` for all exponential calculations.

4.1. Kernel 1

The first kernel is trivial. Each thread is assigned an index of (s, l) , loads its elements of $\sigma_{s,l}$ and $\Delta\lambda_l$, and saves the product. This calculation is not affected by the number of cells and always takes negligible time.

4.2. Kernel 2

The second kernel calculates the heating luminosity $L_{h;c,s}$. Looking at Equation 6, it can be seen that this operation actually is a matrix multiplication of $(\sigma\Delta\lambda)_{s,l}$ and $I_{c,l}$. Each thread is assigned an index of (c,s) and calculates one element of $L_{h;c,s}$. To minimize loads from global memory, the threads in the block first stage blocks of $(\sigma\Delta\lambda)_{s,l}$ and $I_{c,l}$ for an interval in l in shared memory. Each thread then performs the partial sum in Equation 6 for the interval in l that has been staged. The threads then continue to stage another interval in l until the full range in l has been processed. The matrix multiplication example

is extensively discussed in the CUDA Programming Guide (NVIDIA Corporation, 2009b).

4.3. Kernel 3

The third kernel, which solves for the equilibrium temperature $T_{e;c,s}$ is the most complex and time-consuming one. Each thread is assigned an index (c, s) and, since grains with the same s in different grid cells can share the same cross-section data, it is advantageous for each block to process one grain species over many grid cells. This is only possible as long as the entire cross section vector for one grain species can fit in the 16kb of shared memory, which currently limits the maximum number of wavelengths to ~ 4000 . (This limit is of no practical consequence at this time.)

Each thread then loads its value of the heating $L_{h;c,s}$ and calculates a Newton-Raphson iterative solution of Equation 7. The iteration is stopped when the energy non-conservation in Equation 7 is below a specified fraction, currently 0.1%.

The number of iterations required is a strong function of the accuracy of the initial guess for the grain temperature, and because the temperature calculation dominates the total computational time (both on the GPU and CPU) this determines the total time of the calculation. To determine a good guess, the relation between L_h and T_e was studied, for both graphite, silicate and PAH grains. It was found that, for these types of grains, a function of the form

$$\log T \approx k + \beta_1 x + \beta_2 x^2, \text{ where} \quad (11)$$

$$x = \log L_h + \alpha_1 \log a + \alpha_2 \log^2 a, \quad (12)$$

where a is the grain size, can be used to provide the initial guess. Fitting to the grain cross sections resulted in parameters $k = 1.86$, $\beta_1 = 0.189$, $\beta_2 = 3.41 \times 10^{-3}$, $\alpha_1 = -1.39$, and $\alpha_2 = 0.126$ (in SI units). With Equation 11 as the initial guess, the number of iterations required to obtain the temperatures of graphite and silicate grains were at most 7, for any grain temperature below 1000K. The PAH grains sometimes require more iterations, but no more than 9. The exception was that if Equation 11 suggested a temperature of less than 5K, 5K was used. This is due to the convergence behavior of the iteration, which can be unstable at low temperatures if the initial guess is lower than the equilibrium temperature.

Since the number of iterations required to obtain a solution of required accuracy may vary between the threads in the block, the threads may *diverge*. In these cases, execution of the divergent threads is automatically serialized by the hardware. In this case, the threads that require fewer iterations will automatically pause and wait for the thread that takes the longest. It is thus advantageous to make sure the initial guess is good enough that the number of iterations required for the different threads in a warp are all roughly similar, but there is no need to handle this divergence explicitly in the code.

4.4. Kernel 4

The final part of the calculation is the generation of the total dust emission SED in the grid cells from the equilibrium temperatures using Equation 10. Because this kernel uses many different quantities, it has the most complicated shared-memory staging. Each thread is indexed by (c, l) and calculates $L_{\lambda,e;c,l}$. The sums over s are then done by staging blocks of $\sigma_{s,l}$, $T_{e;c,s}$, and n_s for the interval in s covered by the block in shared memory. The layout of this calculation is thus largely similar to that of kernel 1. After the sum is completed, the final quantity is obtained by multiplying by $m_{d;c}$. (Since each value of $m_{d;c}$ is only used once, there is no point in staging it in shared memory.)

After the kernels have finished executing, the resulting SED array is copied back to system memory and, for the purpose of the test presented here, compared with the SEDs calculated on the CPUs.

5. Results

The results presented here compare the CUDA calculation, performed on an Nvidia Tesla C1060 high-performance computing card with 4GB of memory using CUDA version 2.3, to that performed on an 8-core Intel Xeon E5420 (2.5 GHz) Linux machine with 32 GB RAM. The code used for the measurements in this paper is an improved version of SUNRISE version 3.01², and the CUDA calculation is fully integrated into SUNRISE version 3.02. To make the comparison more fair, the CPU code was tuned to improve cache performance and load balancing, and to use the improved initial guess in Equation 11, though there are surely still improvements that could be made. The radiation intensities and dust masses were taken from the simulation of the Sbc galaxy presented in Jonsson et al. (2009), with a grid containing 590k cells. The dust grains were modeled using the graphite cross sections of Laor and Draine (1993) with 81 size bins and the size distribution of the Milky-Way $R = 3.1$ model from Draine and Li (2007). The wavelength grid contained 968 wavelengths distributed from the Lyman limit to 1000 μm .

5.1. Accuracy

To verify that the results of the CUDA calculation are correct, they were compared against the extensively tested calculation in the standard version of SUNRISE performed on the CPU. The result is shown in Figure 1, which shows the mean and variance, over all grid cells, of the relative SED calculated on the GPU and CPU. Because the SED changes dramatically from one grid cell to another, the comparison was done by weighting the cells by the SED (as calculated on the CPU) in that cell. If this is not done, the large variation in the exponential cutoff at short wavelengths will cause the variance to be dominated by the cells

²The code can be retrieved from the SUNRISE SVN repository under `svn/branches/cuda-paper`, revision 2400.

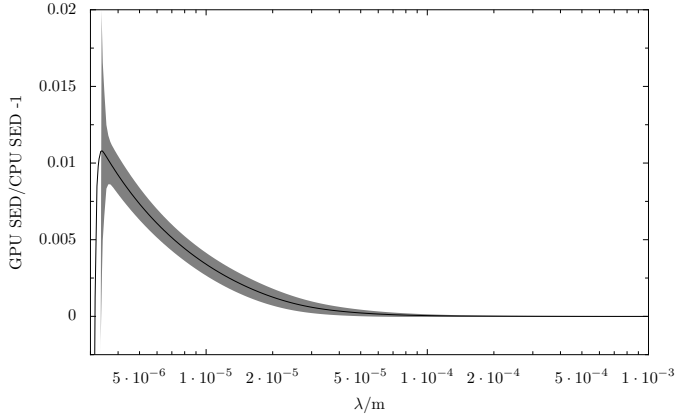


Figure 1: The dust emission SED calculated by the GPU compared to that calculated on the CPU. The line indicates the mean over all cells of the SED ratio, weighted by the CPU SED. The shaded region indicates the 1σ variance (also SED-weighted) over the cells. The blow-up at short wavelengths occurs because the GPU SED is calculated in single-precision and, for the dust temperatures encountered in the problem, the exponential blackbody cutoff will underflow to zero at short wavelengths. This increase in variance at short wavelengths has no practical significance as it occurs precisely because the actual emission drops to negligible levels.

with cold dust – precisely the cells that do not contribute significantly to the total emission. For wavelengths longer than $20\ \mu\text{m}$, where grains in thermal equilibrium can be expected to have an important impact, the difference between the two calculations is about 0.1%, shrinking rapidly at longer wavelengths. The difference increases at shorter wavelengths, reaching 1% at $4\ \mu\text{m}$ and then blowing up as the single-precision exponential cutoff underflows. The 1σ spread around the mean in the results is always negligibly small.

5.2. Performance

To collect performance measurements, the timers in the CUDA runtime library were used to measure the execution times of the different kernels, the total CUDA time (including all kernel runs and data transfer), and the CPU calculation. These data are shown in Table 1 and Figure 2. For large problem sizes, the GPU calculation is 69 times faster than the CPU calculation (on 8 cores). The GPU execution time is dominated by Kernel 3, the numerical temperature solution, which takes 57% of the total time. The time used by the 4 kernels adds up to only 79% of the total GPU time, the remaining time being data transfer to and from the device.

Using the CUDA Visual Profiler (v2.3), the occupancy and memory bandwidth of the kernels were determined. Kernels 1 & 2 have full occupancy, while kernels 3 and 4 have occupancies of 0.5. The time-dominating kernel 3 is not very sensitive to the occupancy, as it is not memory-bandwidth limited. The global memory bandwidth used by kernel 3 is only about 95 MB/s, far below the maximum of 102 GB/s. (This is not surprising, given the fact that

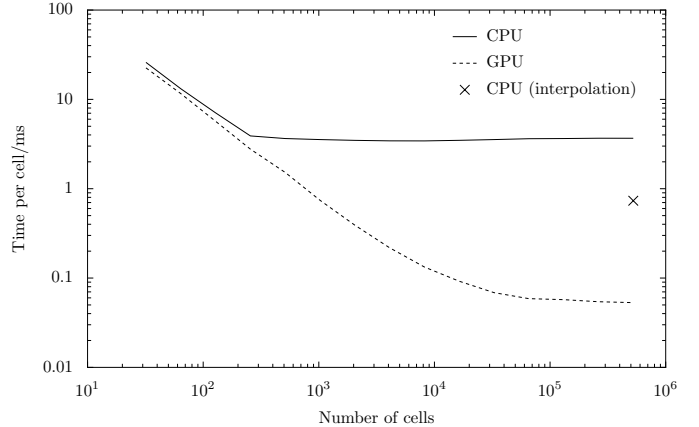


Figure 2: The wall clock time required to calculate the dust emission SED of one grid cell, as a function of the total number of cells, for the CPU (using 8 cores) and GPU. The time when interpolation was used on the CPU is indicated by a point, for the largest number of cells only. This problem used the graphite cross sections of Laor and Draine (1993), with 81 size bins and 968 wavelengths. For small problem sizes, the GPU time is dominated by kernel launch and data transfer overhead and is essentially independent of number of cells up to $> 10^3$ cells. For the CPU calculation, a block size of 32 cells was used, so for 256 cells or less, there are not enough blocks to load all 8 cores, so the time is then independent of problem size. This is merely an artifact of the block size used.

the only per-cell quantities used by kernel 3 are L_h and T_e .)

The instruction throughput of kernel 3 is about 0.7 instructions per cycle, indicating that the threads are not waiting for memory access for a significant amount of time. The throughput would presumably be even higher in the absence of divergent warps. According to the profiler, about 4×10^{-5} of all branches are divergent for this kernel.

6. Discussion

It is clear from the performance numbers presented here that the GPU temperature calculation dramatically outperforms the calculation done on an 8-core fairly modern CPU. This is not very surprising, given that the theoretical maximum floating point performance of the Tesla unit used here is about 6 times greater than that of the 8 Xeon cores. What is more surprising is that the difference in performance actually is an order of magnitude greater than this.

While the large performance difference shows that the calculation performed here is perfectly suited for the massively parallel GPU, one part of the explanation is surely that the CUDA code is a low-level calculation purposely written directly to conform to the rules for getting maximum performance out of the GPU, while the CPU C++ code is written at a much higher abstraction level that largely trusts that the compiler can generate efficient code from the Blitz++ expression template matrix library (Veldhuizen, 1998) and that the CPU cache machinery can hide

No. of cells	GPU	Kernel 1	Kernel 2	Kernel 3	Kernel 4	CPU	Speedup	CPU (interpolation)
32	0.72	$5.7 \cdot 10^{-5}$	$1.4 \cdot 10^{-4}$	$6.4 \cdot 10^{-3}$	$2.7 \cdot 10^{-4}$	0.83	1.2	
64	0.74	$5.7 \cdot 10^{-5}$	$1.5 \cdot 10^{-4}$	$6.7 \cdot 10^{-3}$	$4.4 \cdot 10^{-4}$	0.84	1.1	
128	0.73	$5.8 \cdot 10^{-5}$	$2.4 \cdot 10^{-4}$	$7.6 \cdot 10^{-3}$	$8.1 \cdot 10^{-4}$	0.90	1.2	
256	0.71	$5.8 \cdot 10^{-5}$	$3.8 \cdot 10^{-4}$	$1.2 \cdot 10^{-2}$	$1.5 \cdot 10^{-3}$	1.0	1.4	
512	0.78	$6.0 \cdot 10^{-5}$	$7.0 \cdot 10^{-4}$	$2.0 \cdot 10^{-2}$	$3.0 \cdot 10^{-3}$	1.9	2.4	
1024	0.76	$6.7 \cdot 10^{-5}$	$1.2 \cdot 10^{-3}$	$3.5 \cdot 10^{-2}$	$6.0 \cdot 10^{-3}$	3.6	4.8	
2048	0.80	$8.1 \cdot 10^{-5}$	$2.4 \cdot 10^{-3}$	$6.8 \cdot 10^{-2}$	$1.2 \cdot 10^{-2}$	7.1	8.9	
4096	0.89	$8.8 \cdot 10^{-5}$	$4.8 \cdot 10^{-3}$	0.13	$2.4 \cdot 10^{-2}$	14	16	
8192	1.1	$8.7 \cdot 10^{-5}$	$9.4 \cdot 10^{-3}$	0.26	$4.7 \cdot 10^{-2}$	28	26	
16384	1.5	$8.7 \cdot 10^{-5}$	$1.9 \cdot 10^{-2}$	0.51	$9.5 \cdot 10^{-2}$	57	38	
32768	2.2	$8.7 \cdot 10^{-5}$	$3.7 \cdot 10^{-2}$	1.0	0.19	116	52	
65536	3.9	$8.8 \cdot 10^{-5}$	$7.5 \cdot 10^{-2}$	2.0	0.42	238	62	
131072	7.5	$9.1 \cdot 10^{-5}$	0.15	4.0	1.4	478	64	
262144	14	$8.6 \cdot 10^{-5}$	0.30	8.0	2.8	963	68	
524288	28	$8.8 \cdot 10^{-5}$	0.60	16	5.5	1925	69	385

Table 1: Execution wall clock times, in seconds, of the GPU and CPU (on 8 processors) calculations for different problem sizes. The times are averages of 3 runs. (The kernel execution times were generally very stable, while the times that include data transfer and CPU showed larger variation, presumably due to OS background tasks. The large start-up cost of the GPU calculation is evident. These numbers were obtained for calculations of graphite grains, but the results were approximately the same if silicate and PAH cross sections were used.

memory latency. The performance comparisons presented here thus say less about the innate performance difference between the two architectures and more about the speedups that are possible when a small part of an existing code is rewritten for maximum performance. It is likely that the performance of the CPU code could be further improved by rewriting the CPU calculation to the same low level as the CUDA code, meticulously paying attention to cache performance and blocking the loops to make sure cache thrashing is avoided. The virtue of the GPU memory access scheme, however, is that the rules are simple and straightforward. Knowing exactly how caches, prefetchers, etc., work on any given CPU is much more difficult, but even if cache performance on the CPU was optimal, there is no way the CPU calculation could outperform the GPU. This is especially true given the heavy use of exponentials in the calculation, since the GPU can calculate an exponential in a single clock cycle.

As mentioned earlier, the SUNRISE temperature calculation in production runs is actually done using a linear interpolation table, containing 2000 temperature points between 3 K and 1500 K. The time required is shown in the final column of Table 1. Remarkably, calculating the SED on the GPU is *still more than an order of magnitude faster* than when interpolating the temperature on the 8 CPU cores. This is not quite as unexpected as it might seem, however. Even if the temperature is obtained in zero time, it is necessary to first calculate the heating rate. Subsequently, the emission SED must be calculated using Equation 10. It can be seen from Table 1 that, on the GPU, the temperature calculation (kernel 3) takes about 70 percent of the total execution time. For the CPU code, this fraction is 80 percent, so completely eliminating the temperature calculation can only speed up the CPU calculation by maximally a factor of 5. The actual reduction

in time by using the interpolation on the CPU is indeed very close to 80 percent, which leaves the GPU still more than an order of magnitude faster.

One interesting point is that once a problem has been formulated to fit into the CUDA programming model, scaling to future generations of hardware is virtually ensured. As the calculation already has been subdivided into independent blocks, these blocks can simply be distributed across a larger number of multiprocessors with essentially perfect scaling.

How does the experience here apply to the (much more computationally intensive) calculation of thermally fluctuating grains? In contrast to the calculation here, calculating the temperature probability distribution of thermally fluctuating grains essentially requires inverting a matrix for each grain species (Guhathakurta and Draine, 1989), the size of which is determined by the number of temperature levels in the distribution. If each thread still calculates the temperature distribution of a specific cell and grain species, shared memory use will increase from storing $\sigma_{a;s,l}$ to also storing the full transition matrix between the temperature levels for that grain species. Storing the elements of the temperature probability distribution during the calculation will also require more thread-local storage, potentially increasing the use of bandwidth to global memory. More work needs to be done to determine the best way to implement this calculation on the GPU, and this will be presented in a future paper.

7. Summary

We have presented an implementation of the calculation of dust grain equilibrium temperatures in CUDA, and compared the performance of this implementation running on a GPU with that performed on a normal multicore

CPU. The GPU vastly outperforms the 8 CPU cores, with a factor of 69 speedup. This is almost two orders of magnitude faster despite the fact that the difference in theoretical maximum floating-point performance is only a factor of 6, showing that the inherently parallel, exponential-heavy nature of the calculation is perfectly suited to the GPU. As grain temperature calculations, not the actual transfer of radiation, are normally the most computationally expensive part of calculating the SED of a galaxy, this holds great promise for accelerating such calculations.

8. Acknowledgements

The Nvidia Professor Partnership Program kindly donated a Tesla C1060 in support of this project, and we thank David Luebke, Chris Henze, and Chris Hayward for discussions about how to port various parts of SUNRISE to GPUs. We also thank the anonymous referee for constructive comments that helped both the clarity of the presentation and the efficiency of the calculation. PJ was supported by Spitzer Theory Grant 30183 from the Jet Propulsion Laboratory and by programs HST-AR-10958 & -11758, provided by NASA through grants from the Space Telescope Science Institute, which is operated by the Association of Universities for Research in Astronomy, Incorporated, under NASA contract NAS5-26555.

References

Belleman, R. G., Bédorf, J., Portegies Zwart, S. F., Feb. 2008. High performance direct gravitational N-body simulations on graphics processing units II: An implementation in CUDA. *New Astronomy* 13, 103–112.

Bianchi, S., Oct. 2008. Dust extinction and emission in a clumpy galactic disk. An application of the radiative transfer code TRADING. *A&A*490, 461–475.

Chakrabarti, S., Whitney, B. A., Jan. 2009. Panchromatic Spectral Energy Distributions of Dusty Galaxies with RADISHE. I. Predictions for Herschel: Correlating Colors with Galactic Energy Sources. *ApJ*690, 1432–1451.

Draine, B. T., Li, A., Mar. 2007. Infrared Emission from Interstellar Dust. IV. The Silicate-Graphite-PAH Model in the Post-Spitzer Era. *ApJ*657, 810–837.

Ford, E. B., May 2009. Parallel algorithm for solving Kepler’s equation on Graphics Processing Units: Application to analysis of Doppler exoplanet searches. *New Astronomy* 14, 406–412.

Gaburov, E., Harfst, S., Portegies Zwart, S., Oct. 2009. SAPPORO: A way to turn your graphics cards into a GRAPE-6. *New Astronomy* 14, 630–637.

Gordon, K. D., Misselt, K. A., Witt, A. N., Clayton, G. C., Apr. 2001. The DIRTY Model. I. Monte Carlo Radiative Transfer through Dust. *ApJ*551, 269–276.

Guhathakurta, P., Draine, B. T., Oct. 1989. Temperature fluctuations in interstellar grains. I - Computational method and sublimation of small grains. *ApJ*345, 230–244.

Jonsson, P., Oct. 2006. SUNRISE: polychromatic dust radiative transfer in arbitrary geometries. *MNRAS*372, 2–20.

Jonsson, P., Groves, B., Cox, T. J., Jun. 2009. High-Resolution Panchromatic Spectral Models of Galaxies including Photoionisation and Dust. *MNRAS*, in press (ArXiv:0906.2156).

Laor, A., Draine, B. T., Jan. 1993. Spectroscopic constraints on the properties of dust in active galactic nuclei. *ApJ*402, 441–468.

Li, Y., Hopkins, P. F., Hernquist, L., Finkbeiner, D. P., Cox, T. J., Springel, V., Jiang, L., Fan, X., Yoshida, N., May 2008. Modeling the Dust Properties of $z \sim 6$ Quasars with ART²-All-Wavelength Radiative Transfer with Adaptive Refinement Tree. *ApJ*678, 41–63.

Misselt, K. A., Gordon, K. D., Clayton, G. C., Wolff, M. J., Apr. 2001. The DIRTY Model. II. Self-consistent Treatment of Dust Heating and Emission in a Three-dimensional Radiative Transfer Code. *ApJ*551, 277–293.

NVIDIA Corporation, 2009a. CUDA C Programming Best Practices Guide 2.3.

NVIDIA Corporation, 2009b. CUDA Programming Guide 2.3.

Ord, S., Greenhill, L., Wayth, R., Mitchell, D., Dale, K., Pfister, H., Edgar, R., Sep. 2009. Graphics Processing Units for Data Processing in the Murchison Wide-field Array. In: D. A. Bohlender, D. Durand, & P. Dowler (Ed.), *Astronomical Society of the Pacific Conference Series*. Vol. 411 of *Astronomical Society of the Pacific Conference Series*. pp. 127–+.

Portegies Zwart, S. F., Belleman, R. G., Geldof, P. M., Nov. 2007. High-performance direct gravitational N-body simulations on graphics processing units. *New Astronomy* 12, 641–650.

Veldhuizen, T. L., 1998. Arrays in Blitz++. In: *Proceedings of the 2nd International Scientific Computing in Object Oriented Parallel Environments (ISCOPE’98)*. pp. 223–230.

Weingartner, J. C., Draine, B. T., Feb. 2001. Dust Grain-Size Distributions and Extinction in the Milky Way, Large Magellanic Cloud, and Small Magellanic Cloud. *ApJ*548, 296–309.